Magnetohydrodynamic-Driven Design of Microscopic Endocapsules in MRI

T. Stan Gregory, *Student Member, IEEE*, Kevin James Wu, Jasper Yu, *Student Member, IEEE*, James Brent Box, Rui Cheng, *Student Member, IEEE*, Leidong Mao, Guoyi Tang, and Zion Tsz Ho Tse

***Abstract*—Microscopic medical robots capable of translating in a bloodstream or similar liquid represent a new type of therapeutic technology for surgical interventions. This study aims to characterize a new MRI compliant method of propulsion for swimming robots using the magnetohydrodynamic effect (MHD). An MHD drive is a method of propulsion employing only electromagnetic elements, without the need for moving mechanical parts. By utilizing MHD voltages induced within the MRI magnetic field, the opportunity to propel a device and provide imaging simultaneously is presented. We hypothesized that a wireless MHD-driven thruster could be developed to control endocapsules within the MRI magnetic field. A model capsule was constructed and evaluated in a scaled MRI-environment, and subsequently, tested for MRI-compatibility at 3 T. Dynamic performance of the endocapsule was characterized as input power was varied. In the scaled MRI environment, a peak force of 0.31 mN was observed, providing evidence that an MHD-driven endocapsule is possible in an MRI environment. Increased forces will be obtainable with increases in magnetic field strength and applied power.**

***Index Terms*—Endocapsule, magnetohydrodynamics, magnetic resonance imaging, MRI-compliant, robotic.**

I. Introduction

MICROSCOPIC endocapsules capable of bloodstream navigation represent a new type of therapeutic technology for vascular interventions. With physical dimensions less than a cubic millimeter, microrobots may easily traverse through most vasculature, reaching body regions inaccessible by the conventional surgical practice [1], [2]. A major obstacle in the design of such a capsule is the development of an accurate wireless control method, allowing for intelligent navigation of the endocapsules through the circulatory system. Intelligent navigation would necessitate a coupling of wireless manipulation and advanced imaging technologies, allowing the capsule to precisely locate, advance to, and address obstructions and objectives within the vascular pathway.

Current methodologies cite the usage of varying and rotational magnetic fields as an effort to generate helical movements propelling the capsule forward, backward, and bilaterally [3]. These magnetic-field-based robots do not offer a method to individualize commands to multiple robots, and therefore, are limited to navigating only one capsule in the region of interest. Furthermore, the equipment used to apply the magnetic fields may not be compatible with conventional imaging modalities (magnetic resonance imaging (MRI), computed tomography (CT), positron emission tomography (PET), and ultrasound), which provide necessary information for robust remote navigation and manipulation. Simultaneous imaging and control is necessary in the design of a microsurgical system, as it allows for the monitoring of the target tissue, and accurate localization of the endocapsule.

Similar endocapsule propulsion methods include electrostimulation of surrounding musculature to induce contractions and propel the capsule [4]. These capsules are limited in body regions that can be effectively traversed, and operate with only on-board video cameras; not being designed to work with advanced imaging technologies. Alternative, traditional robotics techniques have been employed, using hybrid locomotion and legged actuation [5]. These methods are also limited in body regions they may traverse due to size constraints, also the presence of an internal magnetic field for the hybrid drive prevent it from coupling well with imaging technologies such as MRI.

Using MHD effect, the external magnetic field and radio-frequency (RF) energy can be employed in a wireless power transfer (WPT) schema to develop a miniaturized endocapsule robot, capable of participating in diagnostic and surgical interventions when tools are integrated within a steerable capsule. Through the transfer of RF energy into the endocapsule using frequency-tuned resonant circuits and the use of static magnetic field in an MRI scanner, we hypothesized that a controllable MHD force can be generated, allowing for the remote manipulation of an endocapsule in the MRI environment.

II. Theory

A. Electromagnetic Propulsion Sources

Motivated by the large amount of high frequency and magnetic energy available through designing endocapsules for usage within the MRI bore, and the high-resolution images that are easily available through MRI, several attempts have been made to make robotic actuators that are MRI-compliant in terms of minimal image SNR reduction, image artifact generation, and electromagnetic interference to the scanner [3], [6]–[8]. These actuators are powered and imaged using the MRI, and are currently in preclinical and phantom stages.

Manuscript received September 23, 2014; revised January 8, 2015; accepted March 3, 2015. Recommended by Technical Editor D. Stoianovici. (*Corresponding author: Zion Tsz Ho Tse.)*

T. S. Gregory, K. J. Wu, J. Yu, J. B. Box, R. Cheng, L. Mao, and Z. T. H. Tse are with the College of Engineering, University of Georgia, Athens, GA 30602 USA (e-mail: stang@uga.edu; kwu@uga.edu; jyu66@uga.edu; chengrui@uga.edu; mao@uga.edu; ziontse@uga.edu).

G. Tang is with the Advanced Materials Institute, Tsinghua University, Shenzhen 518055, China (e-mail: tanggy@sz.tsinghua.edu.cn).

Color versions of one or more of the figures in this paper are available online at http://ieeexplore.ieee.org.

Digital Object Identifier 10.1109/TMECH.2015.2412517

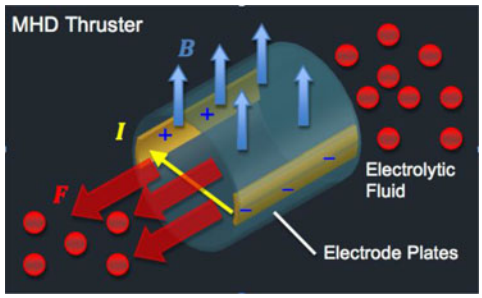

Fig. 1. Translation of the MHD effect into a source of propulsion, and the design of an MHD thruster.

Magnetic gradients produced by the MRI have been programmed for magnetically driven drug delivery to deep-seated human lesions, able to steer an inflow of magnetic microparticles into various phantom model microchannels [6]. Similar preclinical trials have been conducted *in vivo* using rabbit models [7]. MRI-gradient-driven actuators are more commonplace, and have been designed for general intervention in the MRI bore [8]. A surgical biopsy needle has been designed, based on a rotor encapsulating a ferrous sphere, and driven by rotating MRI gradients to fully manipulate the needle [8]. Theoretical simulations have also been performed for miniature swimming endocapsules powered and propelled by the MRI magnetic field, estimating power transfer capabilities using MRI RF energy [3].

These studies have laid appropriate groundwork for the design of an endocapsule propelled using magnetohydrodynamic (MHD) forces under the magnetic field of an MRI, without the use of MRI gradient manipulation, allowing for traditional MRI imaging to be affected by a lesser extent.

B. MHD Propulsion

The MHD force is the induction of a propelling force in flowing conductive fluids when exposed to external magnetic fields. Resultant MHD forces ($\mathrm{F_{MHD}}$) can subsequently be used in the design of microscale devices. A primary focus of $\mathrm{F_{MHD}}$ is in the design of micropumps based on lab-on-a-chip devices for the transport of high ionic strength electrolytic solutions within miniaturized total analysis systems with portable magnetic field generators [9], [10]. $\mathrm{F_{MHD}}$ is directly proportional to the strength of the magnetic field (B_0) and the magnitude of the ionic current (i) over the length (L) of the conductive medium

$$F_{\mathrm{MHD}} = i\,(L \times B). \tag{1}$$

Propulsion is generated through an internal MHD force exerted on the body of the endocapsule (2), stemming from the magnetic flux (B) and current density (J) in the capsule's enclosed volume (V_c). The body force will be largest when the magnetic field and the current approach 90° angles with respect to each other (see Fig. 1)

$$\vec{F}_{\mathrm{MHD}} = \vec{J} \times \vec{B} V_c. \tag{2}$$

In order to define this phenomenon in terms of the external magnetic field, Ohm's law must be employed ($J = \sigma E$) and further modified to include induction, where σ is material conductivity and E is the electric field. Defining E in terms of the Ampere-Maxwell equation (3), and considering displacement currents negligible, yields an alternate representation of the Lorentz Force (4)

$$\nabla \times \vec{B} = \mu_o \left(\vec{J} + \varepsilon_o \frac{\partial \vec{E}}{\partial t} \right) \tag{3}$$

$$\vec{F} = \left(\frac{1}{\mu_o} \right) (\nabla \times \vec{B}) \times \vec{B}. \tag{4}$$

C. Application to Fluid Flow

In order to fully describe the behavior of a flowing fluid under the presence of a magnetic field, the Navier–Stokes equation for an incompressible Newtonian fluid flowing through a pipe (5) provides a simple solution, where ρ is the fluid density, μ_{v} is the viscosity coefficient, v is the fluid velocity, p is the pressure, and f is any external forces

$$\rho \left(\frac{\partial v}{\partial t} + v \cdot \nabla v \right) = -\nabla \rho + \mu_V \nabla^2 v + f. \tag{5}$$

The external force that we are examining is the Lorentz Force (4) and should be substituted into the Navier–Stokes equation to fully describe the system behavior (6). This describes the flow of a conductive fluid when subjected to an external magnetic field, such as arterial blood flow in an MR scanner [11], [12]

$$\rho \left(\frac{\partial v}{\partial t} + v \cdot \nabla v \right) = -\nabla \rho + \mu_V \nabla^2 v + \left(\frac{1}{\mu_o} \right) (\nabla \times B) \times B. \tag{6}$$

From the solution of (6), streamlines generated from the subsequent velocity field can be used to predict the behavior of arterial blood within the boundary conditions generated from the vessel walls. Knowledge of the electric charge of blood plasma can then be used to predict MHD and determine the behavior of an MHD-driven endocapsule in the presence of the MRI magnetic field.

D. Microscale Considerations

The typical inner diameter of human blood vessels varies from 9 μm to 1.5 cm according to different circulatory functions, requiring the device feasibility in the microscale to be considered [13]. Accordingly, the blood stream carried in it has different morphology of the flowing dynamics, of which velocity varies from 0.03 to 40 cm/s [14]. Since our MHD capsule is proposed for medical interventions in a body's vessels, the diameter of capsule D_{cap} should range from 10^{-3} to 1 mm due to the vascular confinement. And the absolute velocity of the capsule v should be larger or at least comparable to the velocity of blood flow $10^{-4} - 10^{-1}$ m/s for manipulation purpose. Considering the density ($\rho = 1.06$ g/cm^3) and the viscosity ($\eta = 3 - 4$ mPa·s) of the human blood [13], the Reynolds number of the MHD capsule in human vessels can be estimated as follows:

$$\mathrm{Re} = \frac{\rho v D_{\mathrm{cap}}}{\eta} \approx 10^{-4}\text{-}10^{2}. \tag{7}$$

From the results in (7), the Reynolds number of the capsule within the human body is low (Re < 0.1) [15]. For simplification, we can convert our model to particle motion in microfluidics

where the capsule is treated as a microparticle with propulsion of the proposed method. And the inertial term in Navier–Stokes (6) is extinct due to the low Reynolds number in the microenvironment [16]. Thus, the motion of the capsule can be derived, whereas by $v_{\rm cap}$ and $v_{\rm fluid}$ represent the velocity of the capsule and near flow, respectively

$$(v_{\rm cap} - v_{\rm fluid})\eta C_{\rm drag} - \vec{F} = 0. \tag{8}$$

$C_{\rm drag} = 3\pi D_{\rm cap}$ is deemed the hydrodynamic drag coefficient proportional to the capsule diameter, and $\vec{F}$ is the Lorentz force exerting on the capsule (1), (2). *I* is the current through the electrolytic fluid between the capsule electrodes of spacing distance $L_{\rm arm}$. *B* is the flux density of the local magnetic field, which can be reorganized into (8), and divided the length of the capsule $L_{\rm cap}$ (9)

$$(v_{\rm cap} - v_{\rm fluid})3\pi\eta - I \times B\xi = 0, \xi = \frac{L_{\rm arm}}{L_{\rm cap}}. \tag{9}$$

Here, *§* is a dimensionless number, depending only on the configuration of the capsule device in different scales. Then, the feasibility of the proposed concept becomes dependent on whether the Lorenz force on the capsule can overcome the hydrodynamic drag force. Furthermore, the bottom line can be estimated for the Lorenz force holding the capsule in the vessels, i.e., $v_{\rm cap} = 0$

$$I \times B \geq \frac{3\pi\eta v_{\rm fluid}}{\xi}. \tag{10}$$

Assuming the configuration dimensions of the capsule prototype (*§*) remains constant when the endocapsule is scaled to the microscale environment, according to (10), there is no explicit impact on performance from the capsule's size. However, the current *I* may be limited by the circuit design inside the microcapsule as well as the electric conductivity. Manipulation of the magnetic field during control perpendicularly to the direction of the current, would also maximize (10), the capsule may hold its maximum predicted velocity with minimal induced current.

Fluid properties, flow rate, and temperature may also produce potential conceptual design issues. Although the electric conductivity of stationary and flowing blood varies with different hematocrit values, it is in the order of $0.1 \sim 1$ S/m [17], a similar order of magnitude as the saline solution currently utilized. Comparing with stationary fluid in the bath of our prototype experiments, the velocity of blood flows has wide range in human body up to blood vessels of different functions. For example, it can be as high as 40 cm/s in aorta, while only 0.3 mm/s in capillary [18]. A further consideration is that blood behaves as a non-Newtonian fluid, with a drag coefficient of its particles approximately proportional to 1/Re [19]. Thus, the drag force in (8) is proportional to the size of the capsule, allow for subsequent conclusions to remain tenable.

The major impact from the temperature inside human body ($\mathrm{T} = 37\,^{\circ}\mathrm{C}$) is the thermal fluctuation to the capsule, however, when the particles are sufficiently small, Brownian motion and diffusion due to thermal fluctuation will affect particle trajectories. For example, when the capsule size $L_{\rm cap}$ approaches the lower boundary of capillary size (1 μm), the mean velocity of the blood flow there is 300 μm/s. According to the Stokes–Einstein relation, $D = \kappa_B T/3\pi\eta D_{\rm cap}$, the diffusion coefficient of the capsule is 1.5×10^{-13} m^2/s. After 20 s of diffusion, the capsule will move an averaged distance of 1.7 μm. Compared with the velocity of the blood stream in capillary, we can neglect the thermal diffusion effect to the capsule manipulation.

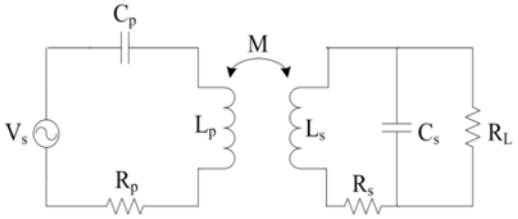

Fig. 2. Delivery of RF energy to the endocapsule through a wireless energy transfer schema.

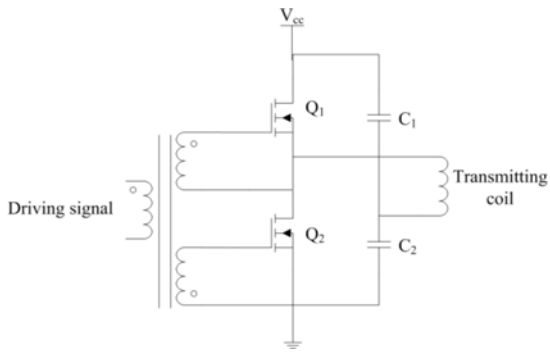

Fig. 3. Output driver for delivery of energy wirelessly to the endocapsule through the primary transmission coil.

III. Methods

A. Wireless Implementation

A WPT schema was developed in order to generate a controllable MHD force within the environment of an MRI scanner, allowing for remote manipulation of an endocapsule using paired frequency-tuned resonant circuits (see Fig. 2).

These resonant circuits will allow for frequency-selectable endocapsules to be manipulated, forming the basis for the design of an MHD-driven endocapsule. The primary coil of the transmitter is driven by a push–pull output driver connected to a waveform generator (see Fig. 3).

The coil can then be capacitively tuned to resonate at the driving frequency $\left(f_r = \frac{1}{2\pi\sqrt{LC}}\right)$. The *Q*-factor, frequency bandwidth of the power transmission relative to the center frequency, of each coil was maximized $\left(Q = \frac{1}{R}\sqrt{\frac{L}{C}}\right)$, while conserving the resonant frequency.

The secondary coil is similarly capacitively tuned such that it is magnetically coupled with the primary power transmission coil circuit; induced signals from different resonant frequencies in the secondary coil are then rectified as shown in Fig. 4.

Using a coil with multiple taps [see Fig. 4(b)], additional rectification and tuning circuits can be added to the capsule, allowing for capsule movements in multiple directions when the secondary coil is excited with different resonance frequencies.

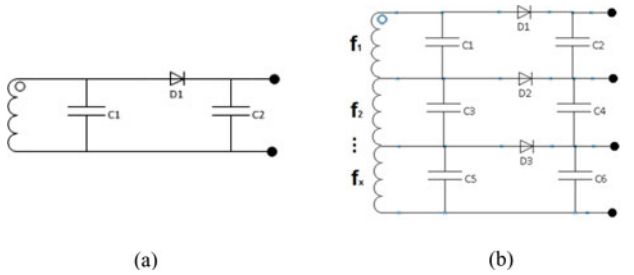

Fig. 4. (a) Single direction rectification circuit for the secondary coil located on the remote endocapsule. (b) Configuration for multidirection control.

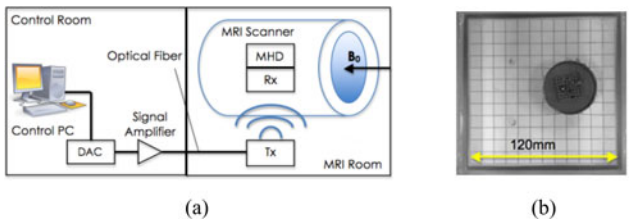

Fig. 5. Experimental design for the quantification of the MHD drive using wireless power delivery. (a) Experimental setup for use of the MHD boat within the MRI bore. (b) MHD boat on 1cm grid used in visual analysis.

An averaging capacitor is used to reduce ripple in the now unipolar signal applied to the MHD copper electrodes, creating a current when placed in an electrolytic solution and producing an MHD force in the presence of the magnetic field. This simplified rectification schema was utilized on the secondary to conserve weight and limit magnetic susceptibility of the capsule.

B. Endocapsule Design

A prototype endocapsule was designed and constructed to evaluate the use the MHD effect as a means of propulsion within a strong static magnetic field. A model capsule (4.27 g) was constructed using an inductive coil and a rectifying circuit mounted upon a 40-mm diameter rapid-prototyped raft. 20-mm nonmagnetic copper plates were used as MHD electrode plates through which a current would be passed. The capsule was placed in a bath of normal saline (0.9% w/v) above a 1-cm grid (see Fig. 5), and in the field of a neodymium magnet (Br max = 0.42 T).

The wireless power transfer scheme depicted in Fig. 2 was used in order to remotely deliver RF energy to the capsule. A primary coil was placed surrounding the saline bath, while a secondary coil was affixed to the capsule, both capacitively tuned to resonate at 1 MHz. A large separation in endocapsule resonant frequency relative to the Larmor frequency of RF energy delivered intra-MRI was selected to minimize device interference with the scanner, thereby reducing change of potential MRI image quality degradation while maintaining endocapsule controllability. WPT efficiency was measured using *S*-parameter characterization with a DB8SAQ Network Analyzer (SDA Kits, Wiltz, U.K.), *S*21 indicated a loss of 0.27 dB and a theoretical efficiency of 94% in wireless energy transfer for the single channel system (11) [see Fig. 6(a)]

$$\text{Gain in dB} = 10\log(\text{Efficiency}) \tag{11}$$

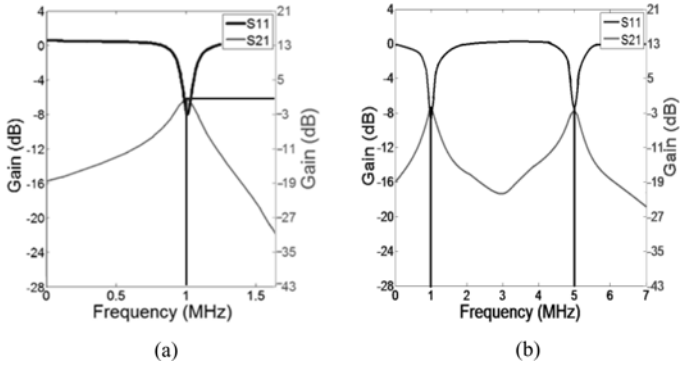

Fig. 6. (a) Quantification of transmitter. (b) Endocapsule receiver coil coupling using *S*-parameters.

Similarly, *S*-parameter characterization was performed for two cascaded rectification circuits, producing a two-channel, multiple direction endocapsule drive [see Fig. 6(b)].

C. Characterization of MHD Drive

Characterization of the MHD drive in the endocapsule prototype was performed using a speed camera. A top view of the saline bath was recorded at 30 fps using a NIKON D5100 video recorder (Nikon Corporation, Tokyo, Japan). Optical tracking was performed using NIH ImageJ Image Processing Software [19] and the MTrackJ utility. Capsule displacement was tracked in each test series as the applied power level was varied and scaled to required power levels at 3 T using (2), yielding a variation of 0–15 W. Four test series were performed as the applied magnetic field strength was varied by increasing electrode displacement from the magnet surface.

Three points were tracked on the capsule at each time point and frames were calibrated using a 1-cm grid overlaid behind the test area. Displacement was recorded and average velocity (v) and acceleration (a) were calculated at each power level using discrete-time differentiation. The MHD force was estimated using capsule mass (m_c) and average acceleration (a_{avg}) (12); kinetic energy (KE) was similarly calculated using peak velocity ($v_{\max}$) (13)

$$F_{\text{body}} = m_c a_{\text{avg}} \tag{12}$$

$$\text{KE} = \frac{1}{2} m_c v_{\max}^2. \tag{13}$$

A predictive model was developed to estimate the propelling force of the capsule based on the difference between the MHD force (2) and the drag force (14) resulting from the movement of the capsule in the saline bath. The capsule was modeled as a streamlined body, and calibrated using experimental data, with a drag coefficient (C_{drag}) of 0.09

$$F_{\text{drag}} = C_{\text{drag}} v. \tag{14}$$

Endocapsule acceleration was calculated directly from this force summation, and velocity was determined through numerical integration. The endocapsule was simulated at each magnetic

Fig. 7. Experimental design for quantification of system performance using enclosed raft design in vasculature surrogate. (a) Sealed endocapsule preliminary design: front view (left) and oblique view (right). (b) Sealed endocapsule in conduit (middle) next to magnet (left) and scale (right).

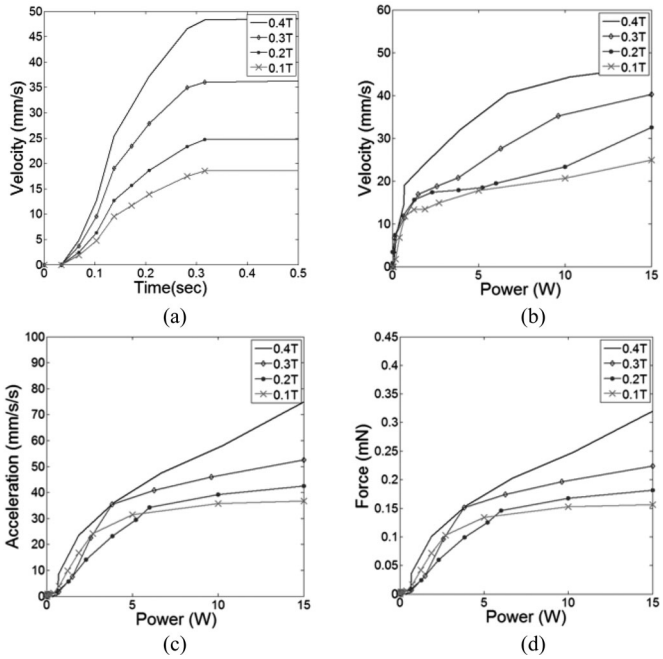

Fig. 8. Quantification of system dynamic performance using the preliminary raft design. Power is scaled to required 3 T levels based on data acquired at lower field strengths. (a) Endocapsule velocity time history at peak input power, (b) peak velocities under varying power levels, (c) endocapsule acceleration, and (d) MHD force.

field strength, with the maximum applied current through the secondary coil.

D. Performance in Enclosed Conduit

In order to quantify the dynamic performance of the endocapsule in an enclosed environment, an enclosed conduit was designed, composed of translucent polyethylene tubing [see Fig. 7(b)]. A tubing diameter of 1.3 cm was chosen, approximately 150% of the endocapsule diameter, and the capsule was tested at the maximum power level from Section III-C. A sealed version of the preliminary raft was designed and rapid prototyped for the purposes of this experiment (see Fig 7), featuring internal housing of integrated electronics and a mass of 1.65 g. The capsule was weighted to neutral buoyancy. Displacement was quantified to determine resultant velocity and acceleration.

E. Evaluation of MR-Compatibility

The compliance of the present endocapsule in the MRI environment was quantified through measurement of both the signal-to-noise ratio (SNR) and the maximum image artifact width generated by the endocapsule [20]–[22]. Image artifact size was defined as a 30% change in pixel intensity in the acquired image before and after the introduction of the introduced endocapsule [23]. SNR was determined to be the ratio of the mean intensity value within a 40 × 40 pixel region located at the image center (I_{center}) and the standard deviation of the intensity values obtained in a 40 × 40 pixel region in the image corner ($\mathrm{SD}_{\mathrm{corner}}$) [24] (15).

$$\mathrm{SNR} = \frac{I_{\mathrm{center}}}{\mathrm{SD}_{\mathrm{corner}}}. \tag{15}$$

The endocapsule was imaged in the isocenter of a 3T-GE SignaHDx MRI (GE Healthcare, Milwaukee, WI, USA) while constrained to a fixed location in a sealed container filled with distilled water using a turbo spin echo (TSE) sequence. TE = 1.8 ms; TR = 5.8 ms. SNR was evaluating using two test conditions: 1) removed capsule from the container (control experiment) and 2) static capsule in the container. The image artifact was evaluated using the subtracted image between 1 and 2 according to ASTM standard.

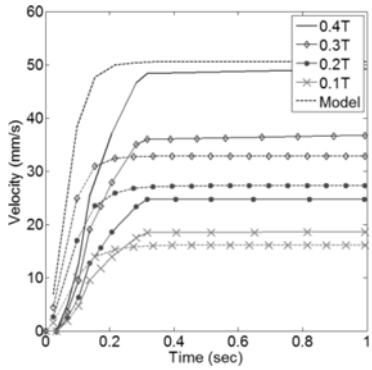

Fig. 9. Comparison of simulated capsule dynamic performance to experimental data.

IV. Results

A. Characterization of MHD Drive

The MHD-driven endocapsule demonstrated a peak velocity of 46.6 mm/s in the test environment, typically accelerating to peak velocity within 0.40 s [see Fig. 8(a)].

A measured peak body force of 0.31 mN was calculated using recorded acceleration data. This illustrates the ability of the MHD effect to propel an endocapsule in a simulated MRI environment. The capsule demonstrated an increase in velocity (and acceleration) with increasing power.

A similar response was observed in the model as compared to experimentally derived datasets. Simulated velocity traces experienced a decreased rise time of approximately 0.1 s (see Fig. 9), attributed to the simplicity of the model.

Steady-state error in model performance was <4% at the highest field strength, with increases in error levels as the velocity and field strength decreased, attributed mainly to differences in the drag force at these levels, left unaccounted for.

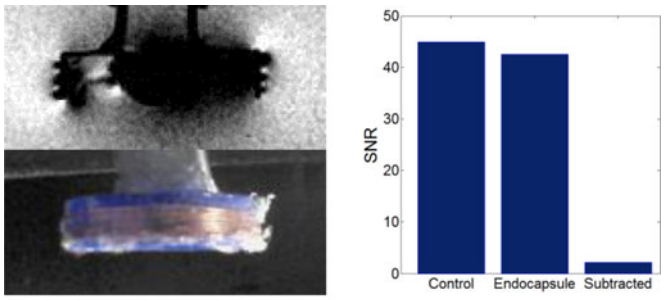

Fig. 10. (a) Measurement of endocapsule MRI compatibility. (b) Evaluation of induced image artifact and signal SNR.

B. Performance in Enclosed Conduit

The MHD-driven sealed endocapsule demonstrated comparable performance in the enclosed conduit with the maximum applied power level from Section III-C. A peak velocity of 33.1 mm/s and an average acceleration of 30.0 mm/s^2 were observed, compared to 46.6 mm/s and 73.46 mm/s^2, respectively, observed in Section III-C. Decreases in average acceleration and peak velocity were attributed to differences in capsule design and increased drag and fluid resistance due to capsule submersion.

C. Evaluation of MR-Compatibility

SNR was calculated for the endocapsule in two test conditions, providing a plane for comparison (see Fig. 10).

A SNR reduction of 5.67% was observed when the endocapsule was introduced into the scanner isocenter and powered on with a maximum power level, which is within an acceptable range of SNR reduction [22], [24], [25]. No observable image artifact can be detected apart from the endocapsule itself.

This experiment suggests that the endocapsule maintains a level of MRI-compatibility and will induce a limited level of image artifacts into the surrounding environment when tested in a surrogate.

V. Discussion

The preliminary model endocapsule provided fundamental evidence that the implementation of an MHD-driven wirelessly powered endocapsule is possible. Using a small test current, the capsule was capable of propelling itself across the test area with a maximum velocity of 46.6 mm/s. Decreases in device size should allow the device to travel at an increased velocity.

Increases in applied power and test current may also lead to increases in resultant velocity. Similar dynamic performance was observed using a sealed endocapsule in the vasculature surrogate, suggesting potential for reliability during submersion. Input power levels will vary due to changes in fluid resistance and with device miniaturization.

The measured resultant forces on the endocapsule were shown to be an order of magnitude greater than similar designs [26], and comparable to later generations [3]. Due to the scaled magnetic field in which this device was tested, it is indicative that with increased magnetic fields, the applied power necessary to generate comparable forces would decrease, whereas the device would maintain the ability to produce larger resultant forces.

The utilization of the MHD effect as the primary mode of propulsion should lead to device robustness to magnetic field inhomogeneity and MRI gradients compared to similar MRI-compliant microdevices due to the method of using applied current rather than variations in magnetic field strength [3], [6].

The device was shown to perform in a closed conduit; however a larger array of test configurations at various fluid velocities must be performed to fully evaluate performance in a true pulsatile vasculature surrogate.

Further development of an active-feedback control schema must be performed in order to effectively navigate in 3-D space. The control algorithm must receive real-time device orientation and position from MRI, such as using passive and active MRI tracking techniques [27], [28], in order to adjust propulsion in each independent direction and maintain a set trajectory.

Steady-state errors in the simulation and the commonality of the observed transient points in the experimental dataset may be attributed to out of plane induced MHD forces, errors in tracking of experimental data, inhomogeneity in the applied magnetic field, and electrical warm-up of the capsule and containing solution.

MRI-compatibility testing at 3 T suggests that the capsule produces a negligible effect on the image SNR when operating during MR scanning. This leads to the conclusion that the device is MRI-complaint in its current configuration.

Limitations in the current model include limited applied field strength relative to that of the MRI magnetic field, which will result in increased resultant acceleration and force. The effects of the generated RF field will need to be examined with regard to subject exposure.

Future work will involve parameter and circuit optimization, and model miniaturization. Further considerations into miniaturization of the resonant circuit and the power transfer schema must also be conducted.

VI. Conclusion

In this study, an MHD drive was designed and evaluated in an MRI-environment, demonstrating the ability to propel a scaled endocapsule in a magnetic field. We characterized two endocapsule designs, and tested the device for MRI-compatibility, indicating its potential as an MRI-compliant microdevice.

Acknowledgment

The authors would like to thank Y. Gao and Dr. Q. Zhao of the University of Georgia, Athens, GA, USA, for their technical advice in coil and RF circuit design.

References

[1] P. Dario, E. Guglielmelli, B. Allotta, and M. C. Carrozza, "Robotics for medical applications," *IEEE Robot. Autom. Mag.*, vol. 3, no. 3, pp. 44–56, Sep. 1996.

[2] D. Stoianovici, C. Kim, G. Srimathveeravalli, P. Sebrecht, D. Petrisor, J. Coleman, S. B. Solomon, and H. Hricak, "MRI-safe robot for endorectal prostate biopsy," *IEEE/ASME Trans. Mechatronics*, vol. 19, no. 4, pp. 1289–1299, Aug. 2014.

[3] G. Kósa, P. Jakab, F. Jólesz, and N. Hata, "Swimming capsule endoscope using static and RF magnetic field of MRI for propulsion," in *Proc. IEEE Int. Conf. Robot. Autom.*, 2008, pp. 2922–2927.
[4] M. Burke, "Bidirectional propulsion of devices along the gastrointestinal tract using electrostimulation," Ph.D. dissertation, Univ. College London, London, U.K., 2013.
[5] M. Simi, P. Valdastri, C. Quaglia, A. Menciassi, and P. Dario, "Design, fabrication, and testing of a capsule with hybrid locomotion for gastrointestinal tract exploration," *IEEE/ASME Trans. Mechatronics*, vol. 15, no. 2, pp. 170–180, Apr. 2010.
[6] J.-B. Mathieu and S. Martel, "Magnetic microparticle steering within the constraints of an MRI system. Proof of concept of a novel targeting approach," *Biomed. Microdev.*, vol. 9, pp. 801–808, 2007.
[7] P. Pouponneau, J.-C. Leroux, G. Soulez, L. Gaboury, and S. Martel, "Co-encapsulation of magnetic nanoparticles and doxorubicin into biodegradable microcarriers for deep tissue targeting by vascular MRI navigation," *Biomaterials*, vol. 32, pp. 3481–3486, 2011.
[8] P. Vartholomeos, L. Qin, and P. E. Dupont, "MRI-powered actuators for robotic interventions," in *Proc. IEEE/RSJ Int. Conf. Intell. Robots Syst.*, 2011, pp. 4508–4515.
[9] A. Homsy, S. Koster, J. C. Eijkel, A. van den Berg, F. Lucklum, E. Verpoorte, and N.F. de Rooij, "A high current density DC magnetohydrodynamic (MHD) micropump," *Lab Chip*, vol. 5, pp. 466–71, Apr. 2005.
[10] P. J. Wang, C. Y. Chang, and M. L. Chang, "Simulation of two-dimensional fully developed laminar flow for a magneto-hydrodynamic (MHD) pump," *Biosens. Bioelectron.*, vol. 20, pp. 115–21, Jul. 30, 2004.
[11] B. Bhatt and M. Reddy, "Theoretical analysis of induced potentials due to blood flow under the static magnetic field of MRI," *Indian J. Biomech.*, pp. 51–55, 2009.
[12] Y. Kinouchi, H. Yamaguchi, and T. S. Tenforde, "Theoretical analysis of magnetic field interactions with aortic blood flow," *Bioelectromagnetics*, vol. 17, pp. 21–32, 1996.
[13] O. M. Pedersen, A. Aslaksen, and H. Vik-Mo, "Ultrasound measurement of the luminal diameter of the abdominal aorta and iliac arteries in patients without vascular disease," *J. Vascular Surg.*, vol. 17, pp. 596–601, 1993.
[14] B. D. Gerard J. Tortora, *The Cardiovascular System. Blood Vessels and Hemodynamics*. New York, NY, USA: Wiley, 2012.
[15] N. L'Heureux, S. Paquet, R. Labbe, L. Germain, and F. A. Auger, "A completely biological tissue-engineered human blood vessel," *Faseb J.*, vol. 12, pp. 47–56, Jan 1998.
[16] P. Gravesen, J. Branebjerg, and O. S. Jensen, "Microfluidics—A review," *J. Micromech. Microeng.*, vol. 3, 1993.
[17] K. R. Visser, "Electric-conductivity of stationary and flowing human blood at low-frequencies," *Med. Biological Eng. Comput.*, vol. 30, pp. 636–640, Nov. 1992.
[18] E. N. Marieb and K. Hoehn, *The Cardiovascular System: Blood Vessels*. New York, NY, USA: Pearson, 2013.
[19] O. M. Sokovnin, N. V. Zagoskina, and S. N. Zagoskin, "Hydrodynamics of motion of spherical particles, drops, and bubbles in non-Newtonian fluid. Numerical methods of investigation," *Theoret. Found. Chem. Eng.*, vol. 46, pp. 464–476, Sep 2012.
[20] M. D. Abràmoff, P. J. Magalhães, and S. J. Ram, "Image processing with ImageJ," *Biophotonics Int.*, vol. 11, pp. 36–43, 2004.
[21] D. Stoianovici, "Multi imager compatible actuation principles in surgical robotics," *Int. J. Med. Robot. Comput Assisted Surg.*, vol. 1, pp. 86–100, 2005.
[22] N. Yu, R. Gassert, and R. Riener, "Mutual interferences and design principles for mechatronic devices in magnetic resonance imaging," *Int. J Comput. Assisted Radiol. Surg.*, vol. 6, pp. 473–488, 2011.
[23] H. Sajima, H. Kamiuchi, K. Kuwana, T. Dohi, and K. Masamune, "MR-safe pneumatic rotation stepping actuator," *J. Robot. Mechatronics*, vol. 24, pp. 820–827, 2012.
[24] ASTM. (2013). F2119 standard test method for evaluation of MR image artifacts from passive implants. [Online]. Available. http://www.astm.org/Standards/F2119.htm
[25] K. Chinzei, R. Kikinis, and F. A. Jolesz, "MR compatibility of mechatronic devices. Design criteria," in *Proc. Med. Image Comput. Comput.-Assisted Intervention*, 1999, pp. 1020–1030.
[26] G. Kósa, M. Shoham, and M. Zaaroor, "Propulsion method for swimming microrobots," *IEEE Trans. Robot.*, vol. 23, no. 1, pp. 137–150, Feb. 2007.
[27] L. Qin, E. J. Schmidt, Z. T. H. Tse, J. Santos, W. S. Hoge, C. Tempany-Afdhal, K. Butts- Pauly, and C. L. Dumoulin, "Prospective motion correction using tracking coils," *Magn. Resonance Med.*, vol. 69, no. 3, pp. 749–759, 2013.
[28] M. Rea, D. McRobbie, H. Elhawary, Z. T. H. Tse, M. Lampérth, and I. Young, "System for 3-D real-time tracking of MRI-compatible devices by image processing," *IEEE/ASME Trans. Mechatronics*, vol. 13, no. 3, pp. 379–382, Jun. 2008.

T. Stan Gregory (S'06) received the B.S. degree in biomedical engineering from the University of North Carolina at Chapel Hill, Chapel Hill, NC, USA, in 2010 and the M.S. degree in biomedical engineering from Virginia Polytechnic Institute and State University, Blacksburg, VA, USA, in 2012. He is currently working toward the Ph.D. degree in biological engineering at the University of Georgia, Athens, GA, USA.

His research interests include the applications of magnetohydrodynamic distortions in recorded electrocardiograms in high field magnetic resonance imaging (MRI), while developing technologies to both improve image quality and lessen time associated with cardiac MRI.

Mr. Gregory received a University Innovation Fellowship in 2015 (National Science Foundation Sponsored EPICENTER), the John Paul Stapp Best Paper Award in 2012 (Stapp Car Crash Conference), and a second place award in the International Student Safety Technology Design Competition in 2011 (National Highway Traffic Safety Administration).

Kevin James Wu is currently working toward the B.S. degree in biological engineering with a focus in bioinstrumentation and medical device design from the University of Georgia, Athens, GA.

His research interests include the study of vasculature fluid dynamics and magnetohydrodynamics.

Mr. Wu received the Center for Undergraduate Research Opportunities Fellowship in 2015 (The University of Georgia) and the University Innovation Fellowship in 2015 (Stanford University).

Jasper Yu (S'12) received the B.S. degree in computer systems engineering from the University of Georgia, Athens, GA, USA, in 2014.

His research interests include software development, hardware design, and medical device prototyping. He is currently working as a Research Assistant at the University of Georgia, Athens, GA.

James Brent Box received the B.S. degree in biological engineering from the University of Georgia, Athens, GA, USA, in 2013.

His research interests include the mechanical design of MRI-compatible devices and rapid-prototyping technologies. He is currently a Junior Engineering Intern at Cooper Surgical, Inc (Trumball, CT).

Rui Cheng (S'15) received the B.S. degree from Tsinghua University, Beijing, China, and the M.S. degree from the University of Minnesota, Minneapolis, MN, USA. He is currently working toward the Graduate degree at the University of Georgia, Athens, GA, USA.

He is a Research Assistant in the Micro and Magnetic BioMEMS group, University of Georgia. His research interests include utilizing magnetic nanotechnology for interventional therapy and medical diagnosis.

Leidong Mao received the B.S. degree in materials science from Fudan University, Shanghai, China, in 2001 and the Master of Science, Master of Philosophy, and Doctor of Philosophy degrees in electrical engineering from Yale University, New Haven, CT, USA, in 2002, 2005, and 2007, respectively.

He is currently an Associate Professor in the College of Engineering, University of Georgia, Athens, GA, USA. His current research interests include nanoscale magnetism and its application in biomedical applications such as cell sorting, single-cell study, droplet microfluidics, hyperthermia, and magnetic nanomanipulations.

Dr. Mao received the NSF Career Award in 2012 and a Young Scientist Award from 13th International Conference of Magnetic Fluids in 2013.

Guoyi Tang received the Ph.D. degree in materials science from The Central Iron and Steel Research Institute, Beijing, China, in 1990.

He is a Professor and an Executive Director of the Advanced Material Institute of the Graduate School, Tsinghua University, Shenzhen, China. He has been working in the field of mechatronics and materials since 1986, and his list of accomplishments in the field has helped establish his reputation among the international scientific community as an outstanding scholar. He served as a Guest Professor in the Institute for Theoretical and Applied Physics, Stuttgart University, Stuttgart, Germany, from 1999 to 2000, and a Visiting Professor in the Mechanical Engineering Department, University of Alaska Fairbanks, Fairbanks, AK, USA, as well as in the Department of Materials Science and Engineering, North Carolina State University Raleigh, NC, USA.

Dr. Tang received several national level awards in China.

Zion Tsz Ho Tse received the Ph. D. degree in mechatronics in medicine from Imperial College London, London, U.K.

He is currently an Assistant Professor in the College of Engineering and the Principal Investigator of the Medical Robotics Lab, University of Georgia (UGA), Athens, GA, USA. Before joining UGA, he was a Research Fellow at Harvard Medical School and Brigham and Women's Hospital. He has been involved in designing and prototyping a broad range of novel analog–digital electronic devices, most of which have been applied in numerous clinical and industrial environments.